

Microtextures and fluid inclusions from vein minerals hosted in the Pillow Lavas of the Troodos supra-subduction zone

D. Quandt, P. Micheuz, W. Kurz, and K. Krenn

INSTITUTE OF EARTH SCIENCES, UNIVERSITY OF GRAZ, NAWI-GRAZ GEOCENTER, HEINRICHSTRASSE 26, A-8010 GRAZ, AUSTRIA

ABSTRACT

This study deals with microtextures and fluid inclusions from veins and vesicles hosted in the Troodos Pillow Lavas that enable a conclusive model for vein formation during the post-magmatic stage of the Troodos supra-subduction zone. Three different types of veins from the Upper and Lower Pillow Lavas are distinguished and imply different modes of fracturing, fluid flow, and precipitation. (1) Syntaxial calcite-, quartz-, and zeolite-bearing veins are interpreted as mineralized extension fractures that were pervaded by seawater. This advective fluid flow in an open system changed later into a closed system characterized by geochemical self-organization. (2) Blocky and (3) antitaxial fibrous calcite veins are associated with host rock brecciation due to hydrofracturing and diffusion-crystallization processes, respectively. Based on aqueous fluid inclusion chemistry with seawater salinities in all studied vein types, the representative fluid isochores crossed with minimum hydrostatic pressure conditions yield vein mineral precipitation temperatures between 180 and 210 °C at 250 bar, independently of the Pillow Lava units. This points to a heat source for the circulating seawater and implies that vein and vesicle minerals precipitated shortly after pillow lava crystallization under dominant isobaric cooling conditions. Compared to previous suggestions derived from secondary mineral parageneses, significant higher temperatures of vein formation in the Troodos Pillow Lavas are proposed.

LITHOSPHERE, v. 10; no. 4; p. 566–578 | Published online 6 June 2018

<https://doi.org/10.1130/L696.1>

INTRODUCTION

The Troodos ophiolite, Cyprus, is one of the best preserved ophiolites and exposes a complete sequence of ultramafic rocks, layered gabbros, isotropic gabbros, sheeted dykes, pillow lavas, and marine sediments representing the uppermost mantle and oceanic crust (e.g., Gass, 1968; Moores and Vine, 1971; Pearce, 2003; Dilek and Furnes, 2009). Previous studies on the Troodos ophiolite focused in most cases on the geochemistry of the pillow lavas, their implications for plate tectonics (e.g., Schmincke et al., 1983; Pearce et al., 1984; Rautenschlein et al., 1985b), and processes related to alteration in oceanic crust (e.g., Gillis and Robinson, 1985, 1990). Based on geochemical analyses of the pillow lavas and sheeted dykes, a supra-subduction zone (SSZ) setting consisting of a mid-ocean spreading ridge above a nascent subduction zone (subduction initiation) followed by a slab-rollback was proposed (Pearce et al., 1984; Dilek and Flower, 2003; Pearce and Robinson, 2010). The detailed post-magmatic structural evolution of the Troodos SSZ, however, is widely unknown. Preceding studies quantified the extent of rotation and uplift (Robertson, 1977; Clube et al., 1985; Morris et al., 1990) and determined the temperature conditions of alteration. Thus, secondary mineral parageneses, oxygen isotope compositions of secondary carbonates, and fluid inclusions (FIs) trapped in vein quartz indicate an abrupt change in alteration temperatures from >300 °C in the Sheeted Dyke Complex to <100 °C in the Pillow Lavas (Spooner and Bray, 1977; Gillis and Robinson, 1990). These

temperatures are linked with alteration processes but lack any structural information on vein and mineral growth.

Mineralized fractures and vesicles hosted in the Pillow Lavas have the potential to record this post-magmatic evolution in the tectonic framework of a SSZ and are useful indicators of paleo-fluid flow through young oceanic crust. Microtextures and crystallographic orientation of vein minerals provide information on the mode of fracturing. The mineralogy of veins and vesicles has important implications for fluid-rock interaction and environmental conditions during precipitation and growth. Fluid inclusions trapped in vein and vesicle minerals give information on the chemistry of the fluid system and fluid density evolution (e.g., Bons and Montenari, 2005, and references therein). Textural features of re-equilibrated fluid inclusions as a result of differences between internal and confining pressures or ambient temperature changes may contribute to the understanding of the post-magmatic isochoric or non-isochoric pressure-temperature (*P-T*) evolution path of the Troodos SSZ (Vityk and Bodnar, 1995).

In this study we present microtextures and fluid inclusion data from fracture-related veins and vesicles of the Troodos Pillow Lavas that shed light on this missing piece of post-magmatic evolution. Both approaches, supported by cathodoluminescence (CL) imaging as well as Raman micro-spectroscopy, contribute to the understanding of conditions of fracturing, fluid flow, vein and vesicle mineral precipitation and growth in the specific Pillow Lava unit. Particular emphasis is put on fluid inclusion petrography and microthermometry in order to analyze the chemical composition of the fluid system, to constrain *P-T* conditions of vein and vesicle mineral formation, and to track a *P-T* evolutionary path of veins and vesicles after

Dennis Quandt  <http://orcid.org/0000-0002-4381-531X>

their formation in a SSZ setting. Since structures of the Troodos ophiolite, including veins and vesicles, lack regional metamorphic overprints and uplift-related deformation (Gass and Masson-Smith, 1963; Moores and Vine, 1971), this approach constitutes an efficient tool in order to decipher post-magmatic microstructural as well as geochemical processes in this SSZ setting.

GEOLOGICAL SETTING AND STRATIGRAPHY

The Troodos massif is part of a chain of Neotethyan ophiolites that extend along the Alpine-Himalayan orogenic system (Dilek and Flower, 2003). The Troodos ophiolite shows a complete and well-preserved pillow-type ophiolitic stratigraphy reflecting a section through oceanic lithosphere (Gass, 1968; Moores and Vine, 1971; Anonymous, 1972) that started to form ca. 92 Ma (Mukasa and Ludden, 1987).

Harzburgites and dunites constitute the base of the Troodos ophiolite and represent the sub-oceanic lithospheric mantle. They are overlain by ultramafic cumulates and gabbros, sheeted dykes and extrusive rocks, which are covered by Cretaceous pelagic sedimentary rocks (Moores and Vine, 1971; Rautenschlein et al., 1985b; Dilek and Furnes, 2009). Doming exposed mantle peridotites and plutonic rocks in the center of the Troodos massif that are enveloped by the Sheeted Dyke Complex and the extrusive volcanic sequence (Wilson and Ingham, 1959; Carr and Bear, 1960; Bear, 1960; Bear and Morel, 1960; Gass, 1960; Bagnall, 1960; Gass and Masson-Smith, 1963) (Fig. 1).

The extrusive volcanic sequence was subdivided into the Basal Group (BG), Lower (LPL), and Upper Pillow Lavas (UPL) (Wilson and Ingham, 1959; Bear, 1960; Bear and Morel, 1960; Gass, 1960). The BG constitutes a transition zone from the Sheeted Dyke Complex into the LPL (van Everdingen and Cawood, 1995). It is composed of altered dykes

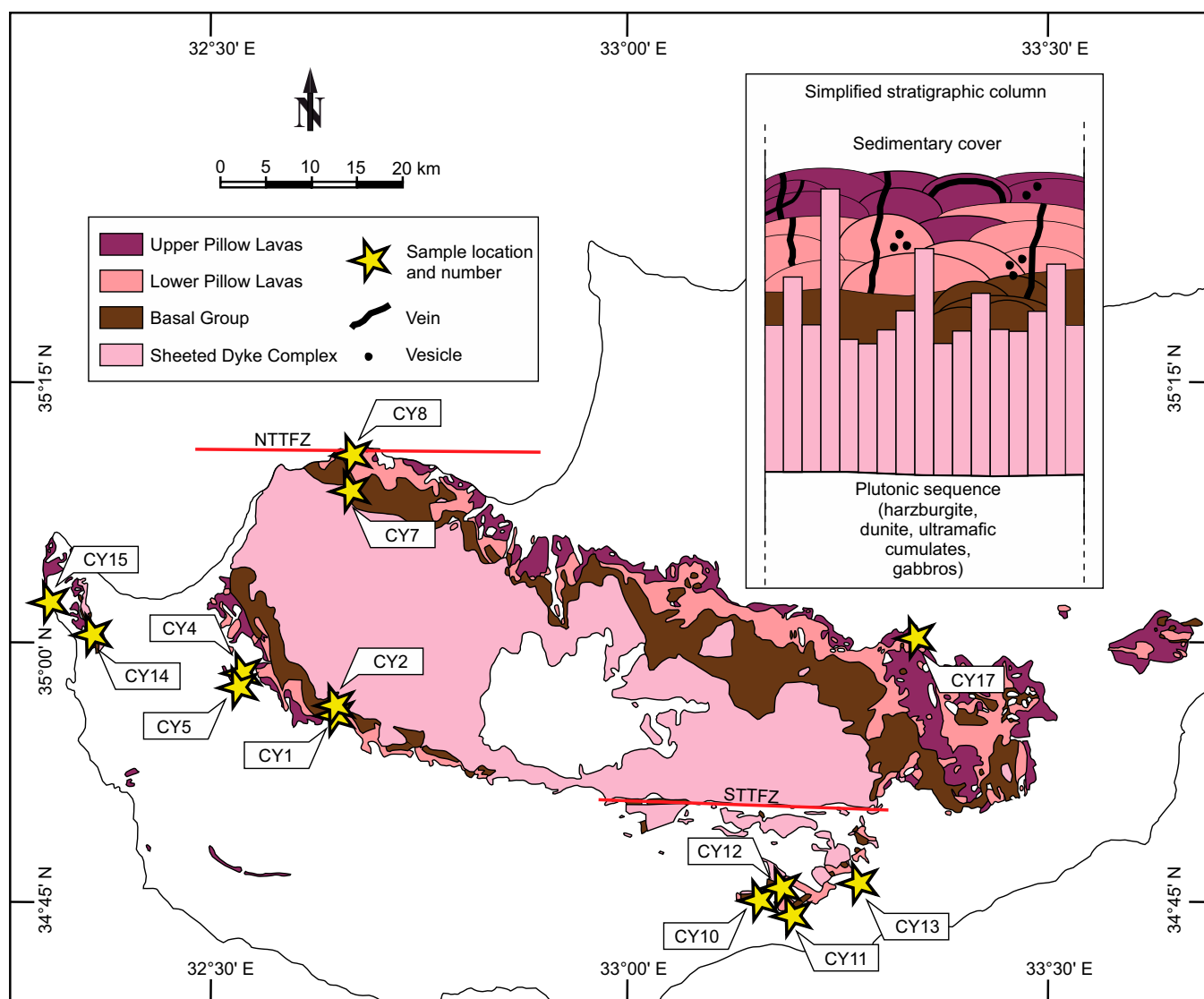


Figure 1. Simplified geological map of the Troodos ophiolite (modified after Constantinou, 1995) and simplified stratigraphic column (modified after Dilek and Furnes, 2009) highlighting the Sheeted Dyke Complex, Basal Group, Lower and Upper Pillow Lavas. NTTfZ and STTFZ refer to the Northern and Southern Troodos (fossil) Transform Fault Zone, respectively (MacLeod and Murton, 1993; Morris and Maffione, 2016). The occurrence of veins and vesicles and their spatial relationships are illustrated in the simplified stratigraphic column. Sites of samples are indicated by yellow stars. See also Table 1 for GPS coordinates of samples and their stratigraphic host rock position.

and pillow lava screens (Bear, 1960). The abundance of dykes, which represent a feeder system for the pillow lavas, decreases from the BG to the UPL (Bear, 1960).

In the Akaki Canyon, an interlayering of evolved andesites and dacites of the LPL with primitive lavas (basaltic andesites) of the UPL is exposed, suggesting a temporal intersection in volcanic activity (Rautenschlein et al., 1985a, 1985b; Thy and Esbensen, 1993). Chemical compositions of pillow lavas and volcanic glasses point to the presence of two lava groups that represent an upper and lower suite (Robinson et al., 1983; Schmincke et al., 1983). The boundary of these two chemically subdivided suites coincides locally with the LPL-UPL boundary described in earlier studies (Wilson and Ingham, 1959; Bear, 1960; Bear and Morel, 1960; Gass, 1960) or appears at some lower stratigraphic levels (Schmincke et al., 1983).

The LPL consist of silicified aphyric basaltic andesites, andesites, and dacites (Bednarz and Schmincke, 1994; Dilek and Furnes, 2009). They are distinguished from the UPL by their high TiO₂ contents and evolved island arc tholeiitic (IAT) character. Volcanic glass compositions show geochemical similarities with the underlying sheeted dykes (Thy and Esbensen, 1993).

The UPL is composed of aphyric and olivine-phyric basalts, andesitic basalts, and picrites (Schmincke et al., 1983; Bednarz and Schmincke, 1994; Dilek and Furnes, 2009). Plagioclase phenocrysts are restricted to basaltic andesites (Rautenschlein et al., 1985b). Low TiO₂, high MgO compositions, and depleted to highly depleted IAT signatures with affinities to boninites are distinct characteristics of the UPL (Robinson et al., 1983; Schmincke et al., 1983; Dilek and Furnes, 2009).

Trace element patterns and the presence of boninites in the extrusive sequence argue for a subduction-related setting (Cameron et al., 1979; Schmincke et al., 1983; Rautenschlein et al., 1985b; Pearce and Robinson, 2010). Thus, the Troodos massif is interpreted as a supra-subduction zone ophiolite in which the Sheeted Dyke Complex and the geochemically related LPL originated from a spreading axis above a nascent subduction zone (Pearce et al., 1984), terminated by two transform fault zones (MacLeod and Murton, 1993; Morris and Maffione, 2016). In contrast, the UPL formed due to subsequent magmatic underplating of the juvenile oceanic lithosphere during subduction initiation in a proto-fore- or back-arc setting (Moore and Vine, 1971; Miyashiro, 1973; Pearce et al., 1984; Thy and Esbensen, 1993; Dilek and Furnes, 2009; Pearce and Robinson, 2010). Pillow lava magmatism commenced ca. 91 Ma and persisted until ca. 75 Ma although ca. 56 Ma old depleted boninite eruptions provide a larger time range (Osozawa et al., 2012). The lack of volcanoclastic material indicates that mature arc volcanism was absent (Robinson et al., 1983).

Between Campanian and early Eocene times, the Troodos microplate rotated 90° anti-clockwise (Clube et al., 1985; Morris et al., 1990). Gypsum and palygorskite veins in the uppermost Pillow Lavas are related to Miocene and renewed Pleistocene uplift of the Troodos ophiolite due to the collision with the Eratosthenes seamount and serpentinization of ultramafic rocks (Robertson, 1977; Gillis and Robinson, 1990; Robertson, 1998).

METHODS

Rock Sampling

Samples of veins and vesicles were taken within the LPL and UPL units (Table 1). Due to the occurrence of pillow lavas in the BG and the absence of a clear upper boundary to the LPL, it cannot be excluded that pillow lavas from the BG were sampled as well. The samples originate from pillow lava outcrops distributed throughout the Troodos ophiolite (Fig. 1). The intention was to sample single veins hosted by preferentially unaltered and undeformed pillow lavas that provide empirically more microstructural and -textural information than veins associated with host rock brecciation or alteration. For consistency, thin and thick sections for vein and host rock petrography, CL, as well as FI study were taken from the same rock chip samples.

Fluid Inclusion Microthermometry

FIs were investigated in double polished thick sections (thickness ~0.15 mm) using a Linkam THSMG600 heating and freezing stage with an operating range from -196 to +600 °C equipped with an Olympus 80x ULWD objective at the NAWI-Graz Geocenter, Institute of Earth Sciences, University of Graz. The Synthetic Fluid Inclusion Reference Set (Bubbles Inc., Blacksburg, Virginia, USA) was used for stage calibration. Temperature measurements are reproducible to 0.2 °C at a heating rate of 0.1 °C/min. The heating-freezing stage was used to obtain eutectic melting temperatures of the aqueous ice phase (IceV → IceLV) [T_e(ice)] as well as final melting of ice (IceLV → LV) [T_m(ice)]. Eutectic temperatures were used to get an approximation of the fluid system after Goldstein and Reynolds (1994). Salinities of the aqueous fluid phase have been calculated using freezing point depression of ice after Bodnar (2003) but also using software Clathrates Q2 (Bakker, 1997). As the last step, total homogenization temperatures T_h (LV → L and/or V) were measured to obtain minimum conditions for the formation of homogeneous trapped FIs by crossing the isochores with an estimated hydrostatic pressure. FI

TABLE 1. SAMPLE LOCATIONS

Outcrop number	Coordinates		Location	Stratigraphic unit
	Latitude (°N)	Longitude (°E)		
CY1	34°56.158'	32°37.501'	Troodos NW-flank	LPL
CY2	34°56.204'	32°37.501'	Troodos NW-flank	LPL
CY4	34°58.638'	32°30.765'	Troodos NW-flank	UPL
CY5	34°57.672'	32°30.479'	Troodos NW-flank	UPL
CY7	35°09.880'	32°37.511'	N-Troodos, interior	LPL/BG
CY8	35°11.490'	32°38.477'	N-Troodos, coast	LPL
CY10	34°45.638'	33°08.105'	S of Arakapas fault, S-Troodos	UPL
CY11	34°46.359'	33°09.801'	S of Arakapas fault, S-Troodos	LPL
CY12	34°44.742'	33°10.432'	S of Arakapas fault, S-Troodos	LPL
CY13	34°46.673'	33°15.172'	S of Arakapas fault, S-Troodos	UPL
CY14	35°00.681'	32°19.838'	NW cape, interior, NW-Cyprus	LPL/BG
CY15	35°02.555'	32°16.613'	NW cape, coast, NW-Cyprus	UPL
CY17	35°01.132'	33°19.277'	Near Margi, E-Troodos	Uppermost UPL (+ LPL?)

Note: Stratigraphic unit is based on the geological map and thin section petrography of host rocks. See also figure 1 for sample location. GPS coordinates refer to WGS84. BG—Basal Group; LPL—Lower Pillow Lavas; UPL—Upper Pillow Lavas.

properties and isochores have been calculated using the software BULK and ISOC, respectively (Bakker, 2003).

Raman Spectroscopy

Raman spectra of minerals were performed in confocal mode using a Jobin Yvon LabRam HR800 microspectrometer equipped with an Olympus BX41 optical microscope and a Si-based CCD (charged-coupled device) detector at the NAWI-Graz Geocenter, Institute of Earth Sciences, University of Graz. The instrumentation uses a 100 mW Nd-YAG laser (532 nm emission), a grating of 1800 grooves/mm, and a slit width of 100 μm . The spectral acquisition time was set to 10–20 seconds for all measurements in the range between 100 and 1200 cm^{-1} for silicate phases but also between 1100 and 3800 cm^{-1} for gases and OH^- phase. Raman spectroscopy was conducted on the same thin sections as used for petrographic and CL study.

Cathodoluminescence Microscopy

The CL study was conducted with a hot cathode CL microscope (Lumic HC5-LM) at the NAWI-Graz Geocenter, Institute of Earth Sciences, University of Graz. Thin sections were polished and carbon coated. Electrons were accelerated with 13–14 kV under a vacuum of $<10^{-5}$ mbar. Beam current varied from 0.2 to 0.6 mA. True-color CL in the visible spectrum was observed and imaged in real time with an attached digital camera.

PETROGRAPHY

Vein Macro- and Microtextures

Based on mineral shapes and microstructures, veins and mineralized vesicles are distinguished using the classification by Bons et al. (2012, and references therein). Veins and vesicles differ in their mineralogy. Structural and textural similarities, however, enable a subdivision into (1) syntaxial veins and vesicles, (2) blocky veins, and (3) antitaxial veins. Textural transitions occur between syntaxial and blocky veins.

Syntaxial Veins and Vesicles

Syntaxial veins occur throughout the whole Troodos ophiolite within the LPL and UPL. They form single veins with relative uniform thickness of ~1–3 mm. Calcite, quartz, and zeolites are the main mineral phases. Samples can be subdivided into completely sealed veins that display a median line and incompletely sealed veins and vesicles with late-stage precipitates (Table 2).

Completely sealed syntaxial veins with a median line. Completely sealed veins of the UPL are pure calcite veins that are characterized

by growth competition between adjacent elongate-blocky crystals and a median line (Fig. 2A). Crystals show strong undulatory extinction, while twinning is rare (type I and II after Burkhard, 1993).

Syntaxial zeolite veins with a median line belong exclusively to the LPL. They are composed of small euhedral tabular heulandite followed by mordenite growth that terminates at the median line (Fig. 2B), or elongate-blocky analcime (Fig. 2C). These zeolites are distinguished by their characteristic Raman spectra (Fig. 3).

Incompletely sealed syntaxial veins and vesicles with late-stage precipitates. Incompletely sealed syntaxial veins of the UPL are composed of blocky to elongate-blocky analcime (Fig. 2D) containing up to three wall rock–parallel solid inclusion bands indicative of repeated crack and sealing events. Non-sealed vein sites are filled with twinned (type I and II twins after Burkhard, 1993) anhedral calcite (Fig. 2D), euhedral acicular natrolite, and blocky analcime that are distinguished by their characteristic Raman spectra (Fig. 3).

The occurrence of incompletely sealed syntaxial quartz veins is restricted to the LPL. Quartz develops euhedral crystal habits. Late-stage anhedral calcite and accessorially goethite precipitated in non-sealed vein sites (Fig. 2E). The proportion between quartz and calcite varies from pure quartz to calcite-dominated veins. Additionally, quartz crystals are located between grain boundaries of late-stage calcite. Late-stage calcite shows type I and II twinning (Burkhard, 1993), and quartz exhibits undulatory extinction.

In large vesicles (up to 25 mm) quartz is coarse grained (up to 10 mm) and has elongate-blocky crystal shapes with undulatory extinction and subgrain boundaries. Quartz precipitation along the vein margins is characterized by growth competition and followed by formation of late-stage quartz in non-sealed sites of the vesicle (Fig. 2F).

Blocky Veins

Blocky veins occur in the LPL as well as UPL and are associated with host rock breccias and branching vein networks. Calcite is the major vein component and develops anhedral blocky crystal aggregates (Figs. 2G–2I, Table 2). Microcrystalline calcite (micrite), euhedral quartz, and angular host rock fragments occur subordinately in some blocky vein samples. Calcite shows undulatory extinction and subgrain boundaries together with type I and II twinning (Burkhard, 1993). Additionally, growth zones are outlined by decrepitated FIs (Fig. 2G). Twin lamellae are partly tapered and slightly bent. Individual euhedral quartz crystals are present along vein margins and between calcite grain boundaries (Fig. 4D).

Antitaxial Veins \pm Median Line

Antitaxial veins occur exclusively in the UPL (location near Margi) where up to 50-mm-thick veins run parallel to each other or branch out and are exposed over several meters along strike. This vein type consists

TABLE 2. VEIN TYPE CHARACTERISTICS

	Syntaxial	Blocky	Antitaxial
Stratigraphic unit	LPL + UPL	LPL + UPL	UPL
Vein and vesicle structure	Single veins and vesicles	Vein breccias and branching veins	Branching veins
Vein and vesicle thickness	1 to 3 mm (veins), 25 mm (vesicle)	1 to 50 mm	0.5 to 50 mm
Vein and vesicle mineralogy	Perfectly sealed: Cal, Anl, Hul, Mor	Imperfectly sealed: Cal, Qtz, Anl \pm Ntr \pm Gth	Cal, \pm Qtz
Mineral shape	Elongate-blocky	Elongate-blocky to blocky, euhedral	Blocky
Vein and vesicle characteristics	Median line, growth competition	Solid inclusion bands	Host rock fragments, micrite
			Fibrous, partly recrystallized Solid inclusion bands, curved fibers, median line relict

Note: Anl—analcime; Cal—calcite; Gth—goethite; Hul—heulandite; LPL—Lower Pillow Lavas; Mor—mordenite; Ntr—natrolite; Qtz—quartz; UPL—Upper Pillow Lavas.

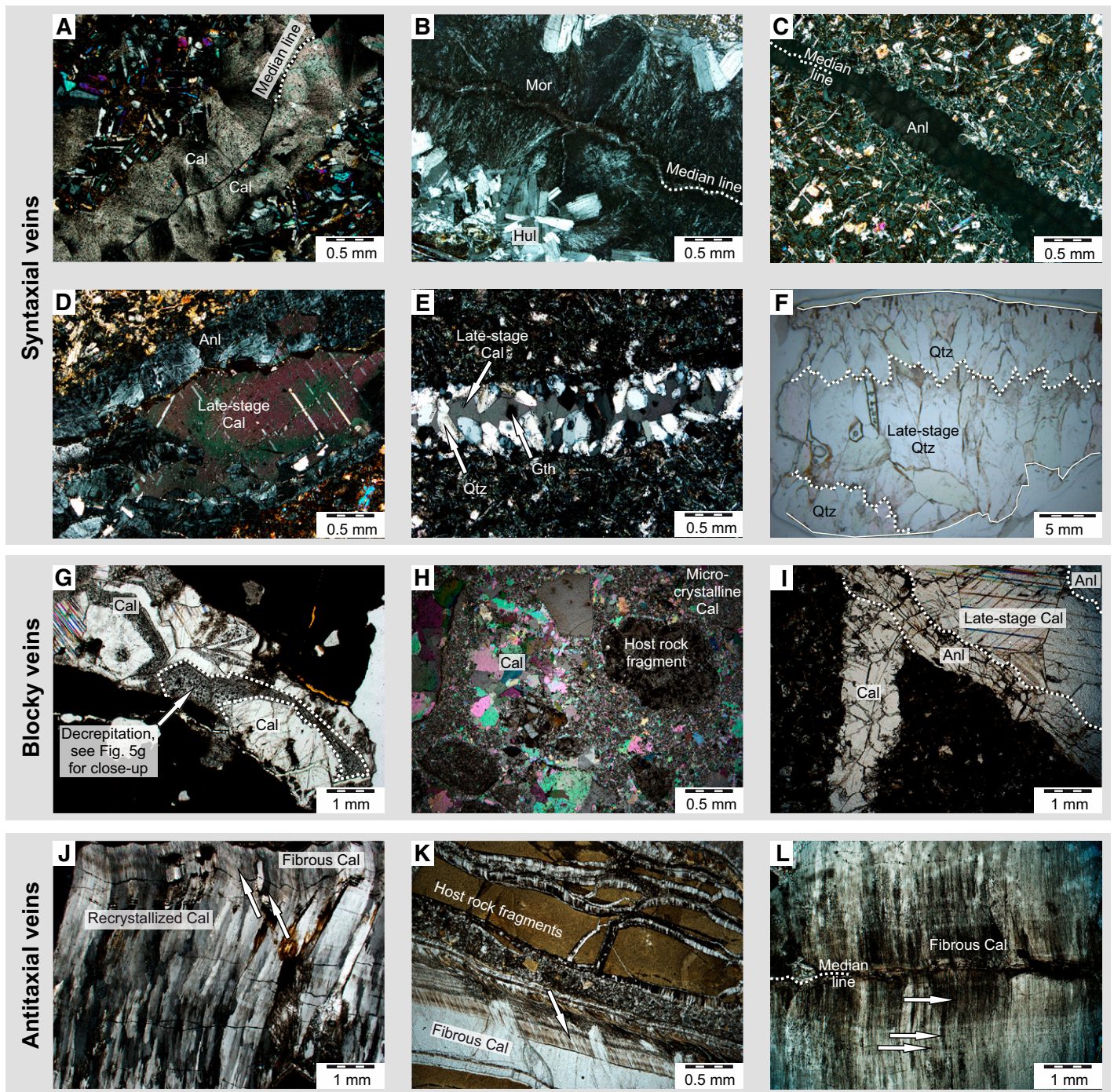


Figure 2. Photomicrographs of all vein types. (A–C) Completely sealed syntaxial veins composed of elongate-blocky calcite (Cal), mordenite (Mor) succeeding heulandite (Hul) and analcime (Anl) whose growth terminates at a median line (# nicols). (D–F) Incompletely sealed syntaxial veins without median line: (D) analcime and late-stage calcite (# nicols), (E) euhedral quartz (Qtz) and late-stage calcite with accessory goethite (Gth, # nicols), and (F) vesicle with elongate-blocky and late-stage quartz (// nicols). (G–I) Blocky calcite veins are characterized by (G) growth zones, best distinguished by inclusion-rich (fluid inclusion [FI] decrepitation, // nicols, see Fig. 5G for close-up of decrepitated FIs) and inclusion-poor domains or (H) microcrystalline calcite and host rock fragments (# nicols). (I) Blocky calcite vein crosscut by incompletely sealed syntaxial analcime vein (// nicols). (J–L) Antitaxial calcite veins (J and L, # nicols, K, // nicols). (J) Curvature of calcite fibers decreases toward the vein center where the fibrous crystal habit is only recognizable as a relict. Fibers contain multiple wall rock-parallel solid inclusion bands (arrows in J, K, and L).

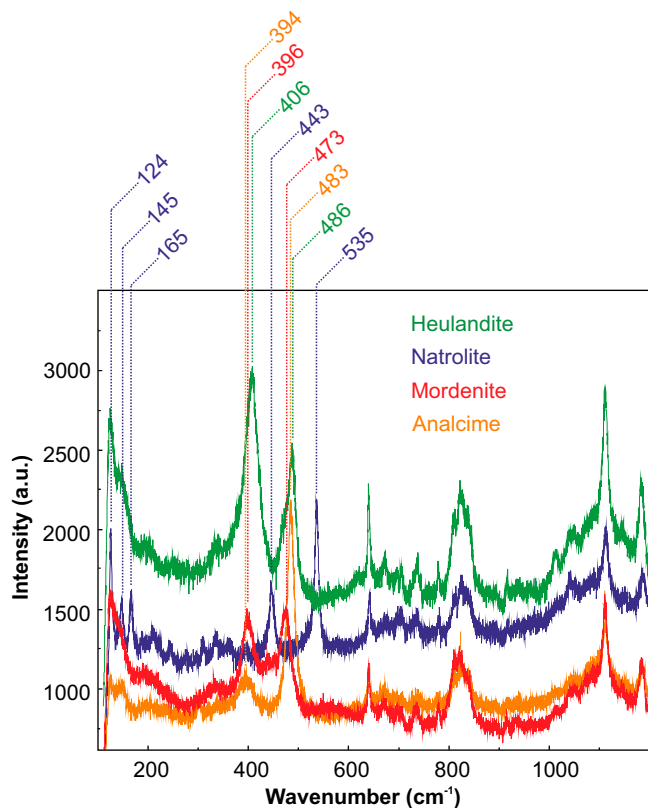


Figure 3. Raman spectra of zeolite minerals. Subdivision after Knight et al. (1989). Peaks >600 cm⁻¹ result partly from epoxy resin.

solely of fibrous calcite that contains multiple wall rock-parallel solid inclusion bands (Figs. 2J–2L; Table 2). Calcite shows undulatory extinction and subgrain boundaries in the center where the fibrous nature is only preserved as a relict, while no twinning is observed. Fibrous calcite displays a curvature that weakens toward the vein center (Fig. 2J).

Cathodoluminescence Microscopy

Elevated ratios between Mn²⁺ (CL activator) and Fe²⁺ (CL quencher) (Fairchild, 1983) cause yellow, orange, and red CL in calcite. In completely sealed syntaxial calcite veins, high-luminescent Mn-rich domains host accumulations of decrepitated FIs, while decrepitation-free areas are nearly non-luminescent and poor in Mn (Fig. 4A). Late-stage calcite from incompletely sealed syntaxial quartz veins shows similarly luminescent areas that are rich in decrepitated FIs (Fig. 4B). Late-stage calcite associated with incompletely sealed syntaxial analcime veins exhibits highly repetitive oscillatory growth zoning, including sectoral and intrasectoral zones and luminescent calcite twins (Fig. 4C).

In blocky veins, calcite displays comparatively broad growth zoning. Mn-rich high-luminescent growth zones, rich in decrepitated fluid inclusions, alternate with Mn-poor low-luminescent fluid inclusion-poor areas (Fig. 4D).

Antitaxial calcite veins show abruptly as well as gradually decreasing CL intensities along fiber growth direction from the median line, which is only visible under CL, toward the margins (Figs. 4E and F). Luminescent bands pervade calcite fibers and appear parallel to the median line (Fig. 4F). Additionally, crosscutting relationships between two antitaxial fibrous calcite veins are visible due to different CL intensities (Fig. 4G).

Fluid Inclusion Study

Quartz, calcite, and analcime from incompletely sealed syntaxial veins including vesicles as well as calcite from blocky veins host suitable FIs for microthermometry. FIs can be texturally subdivided into primary (type A), predominantly arranged as single and clusters, secondary (type B), oriented along intragranular trails and planes, and primary FIs with clear post-entrapment modifications like decrepitation and re-equilibration (type C). This subdivision can be applied to most samples throughout the whole extrusive sequence of the Troodos ophiolite. Type A is the most frequent inclusion type hosted in calcite, quartz, and analcime, while type B is limited to calcite and quartz. Type C occurs in quartz and calcite and is in most cases restricted to growth domains (Fig. 4D).

In general, all FIs consist of two phases (liquid + vapor: L + V) at room temperature and homogenize into the liquid phase, indicative for pressure-dominated inclusions. Eutectic temperatures *T_e*(ice), if observable, lie between -35.0 and -21.2 °C suggesting additional chlorides like NaCl ± KCl ± MgCl₂ in the aqueous solution. Last melting temperatures *T_m*(ice) around -3.3 and -0.4 °C (average value -1.6 °C) point to low salinities around 2.74 mass%, close to seawater salinity (Spooner and Bray, 1977). FIs are distinguished by their density dependent homogenization temperatures *T_h*. FI data from different vein samples are given in Table 3.

Fluid Inclusion Type A

Type A FIs have a size of up to 30 μm and show regular rounded shapes in quartz and straight phase boundaries in calcite (Figs. 5A and 5B). The degree of fill is ~0.90–0.95. Minimum temperature estimates for vein formation are linked with homogenization temperatures *T_h* of primary type A FIs, which show a wide range from 173.6 to 227.3 °C in quartz (peak frequencies between 180 and 190 °C) and 147.3–217.8 °C in calcite (peak frequencies between 190 and 210 °C) (Figs. 6A and 6B). This corresponds to densities in quartz and calcite from 0.85 to 0.92 g/cm³ and from 0.87 to 0.94 g/cm³, respectively. Analcime hosts minor type A FIs (Fig. 5C) with *T_h* ranging from 183.5 to 210.7 °C (Fig. 6C). Corresponding densities are between 0.88 and 0.91 g/cm³.

Fluid Inclusion Type B

Type B FIs are arranged along intragranular (grain boundary to grain boundary or grain boundary to interior) trails and planes (Figs. 5D and 5E) and in general, if not elongated in shape, smaller (in most cases <10 μm) than type A FIs. Elongated FI trails in quartz and calcite, however, reach long axis diameters of 20–30 μm. Degree of fill is almost comparable to type A FIs between 0.90 and 0.95. Minimum temperature estimates of fluid entrapment (*T_h*) for type B FIs lie between 92.0 and 177.5 °C in quartz (two peak frequencies at 115 and 175 °C) and between 90.0 and 176.2 °C in calcite (peak frequency at 165 °C) (Figs. 6A and 6B). This corresponds to a consistent density range between 0.91 and 0.98 g/cm³ for type B in quartz and calcite. No type B FIs were observed in analcime.

Fluid Inclusion Type C

Type C FIs in quartz and calcite are in most cases restricted to inclusion-rich growth domains. In case of calcite, these growth zones can be clearly distinguished from areas containing type A and B FIs by increased CL intensities due to elevated Mn/Fe ratios (Fig. 4D). FIs are large in size (up to 100 μm) and in most cases decrepitated and empty. They occur predominantly as clusters and/or as single inclusions (Figs. 5F–5H). *T_h* range from 197.5 to 239.1 °C in quartz, 219.4–253.0 °C in calcite, and 196.3–262.3 °C in analcime (Figs. 6A–6C). However, due to re-equilibration and density loss, densities are not calculated (Table 3).

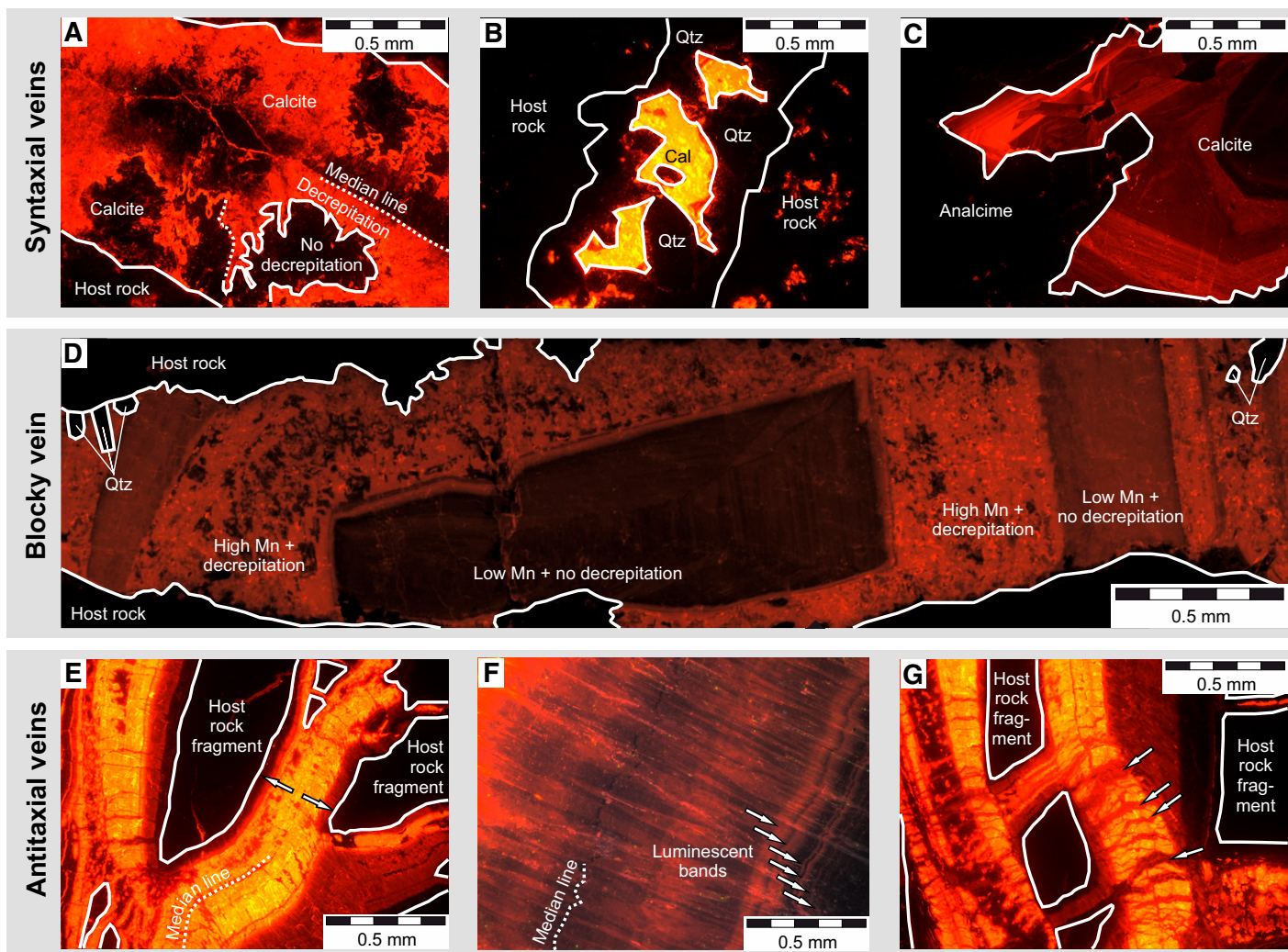


Figure 4. Cathodoluminescence (CL) images of vein types. (A) Calcite from completely sealed syntaxial veins with median line and (B) late-stage calcite (Cal) from incompletely sealed syntaxial veins display high-luminescent areas enriched in decrepitated fluid inclusions (FIs). Qtz—quartz. (C) Late-stage calcite associated with analcime in incompletely sealed syntaxial veins exhibits highly repetitive oscillatory growth zoning with sectoral and intrasectoral zones. (D) In blocky calcite veins, Mn-rich luminescent growth zones enriched in decrepitated FIs alternate with low-luminescent growth zones without decrepitated FIs. (E) Fibrous calcite from antitaxial veins reveals a decrease in CL intensities in fiber growth directions (arrows). Note median lines are only recognizable under CL (E, F). (G) Late calcite generation with low CL intensities crosscuts an earlier calcite generation (arrows).

TABLE 3. MICROTHERMOMETRY DATA OF FLUID INCLUSIONS

Sample	Vein type	Stratigraphic unit	Host mineral	Fluid inclusion type	n	Texture	Size (μm)	Phases	T _h (°C)	Density (g/cm ³)
CY5	Syntaxial vein	UPL	Anl	A	4	Cluster, single	1 to 10	L + V	183.5 to 210.7	0.88 to 0.91
			Anl	C	12	Re-equilibrated cluster, single	5 to 30	L + V	196.3 to 262.3	N.D.
			Cal	A	3	Single	5 to 20	L + V	147.3 to 172.3	0.92 to 0.94
			Cal	B	4	Trails	5 to 20	L + V	90.0 to 139.9	0.95 to 0.98
CY7	Syntaxial vesicle	LPL/BG	Qtz	A	5	Cluster, single	5 to 10	L + V	183.0 to 227.3	0.85 to 0.91
			Qtz	B	31	Trails, planes	5 to 30	L + V	92.0 to 177.5	0.91 to 0.98
CY8	Blocky vein	LPL	Cal	A	39	Single, cluster	5 to 30	L + V	169.4 to 217.8	0.87 to 0.92
			Cal	B	13	Trails, planes	1 to 10	L + V	139.7 to 176.2	0.95 to 0.98
			Cal	C	6	Re-equilibrated cluster, single	5 to 30	L + V	219.4 to 253.0	N.D.
CY12	Syntaxial vein	LPL	Qtz	A	19	Cluster, single	5 to 10	L + V	173.6 to 203.9	0.88 to 0.92
			Qtz	B	9	Trail	1 to 10	L + V	149.0 to 175.5	0.92 to 0.94
			Qtz	C	13	Re-equilibrated cluster, single	5 to 50	L + V	197.5 to 239.1	N.D.

Note: Anl—analcime; BG—basal group; Cal—calcite; LPL—Lower Pillow Lavas; L + V—liquid plus vapor; n—amount of measured fluid inclusions; N.D.—no data; Qtz—quartz; T_h—homogenization temperature; UPL—Upper Pillow Lavas.

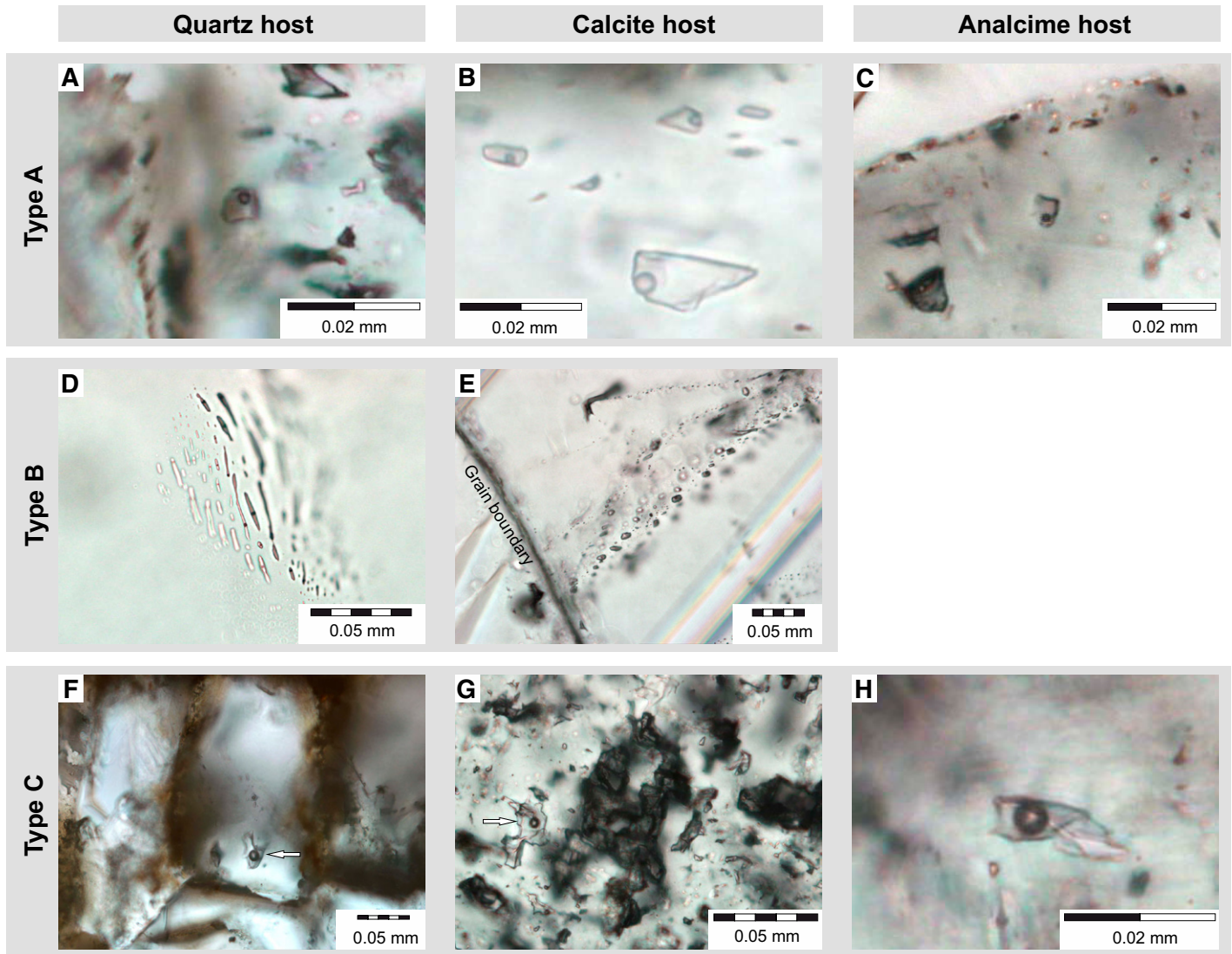


Figure 5. Photomicrographs of type A, B, and C fluid inclusions (FIs) in quartz, calcite, and analcime. (A) Type A FI in syntaxial quartz (host shown in Fig. 2E), (B) blocky calcite (host shown in Fig. 2G), and (C) syntaxial analcime (host shown in Fig. 2D). (D) Elongated type B FIs in late-stage quartz vesicle (host shown in Fig. 2F). (E) Type B FIs in blocky calcite along intragranular trails (host shown Fig. 2G). (F) Large re-equilibrated type C FI in syntaxial quartz vein (arrow, host shown in Fig. 2E). (G) Decrepitated and re-equilibrated (arrow) type C FIs in blocky calcite (host shown Fig. 2G). (H) Re-equilibrated type C FI in syntaxial analcime (host shown in Fig. 2D).

DISCUSSION

P-T Evolution

It is assumed that veining occurs steadily after solidification of newly formed pillow lavas providing sufficient heat for the observed high-temperature precipitates of seawater origin. This implies firstly that veins from the UPL and LPL are not contemporaneous and veining initiated in the LPL before emplacement of the UPL, and secondly solely hydrostatic pressure applies to all host minerals during FI entrapment. The lack of veins in the studied outcrops with consistent mineralogy and microtextures that crosscut the whole volcanic pile supports this assumption.

Pillow lava extrusion spans a wide time range from 91 to 75 Ma with some limited depleted boninite eruptions until 56 Ma along the southwestern flank of the Troodos ophiolite (Osozawa et al., 2012). It

is therefore supposed that veins and vesicles have formed within this temporal framework.

P-T conditions for vein and vesicle mineral precipitation are based on isochore calculations of type A and B FIs combined with a hydrostatic pressure estimate of 250 bar that corresponds to a seawater column of ~2500 m, analog to average mid-ocean ridge depth below sea level (Sclater et al., 1971; Spooner, 1980). This hydrostatic pressure, however, represents a minimum estimate, since it cannot be excluded that ongoing pillow lava emplacement on top of the volcanic pile led to an additional load.

Calculated steep isochores of aqueous type A and B FIs from each vein type represent approximate geothermometers (Figs. 7A–7D). Isochores are constrained by $\pm 20\%$ of the estimated minimum hydrostatic pressure (200 and 300 bar).

Type A FIs entrapped in quartz and calcite from syntaxial and blocky veins of the LPL including vesicles show a clear overlap of *P-T* conditions

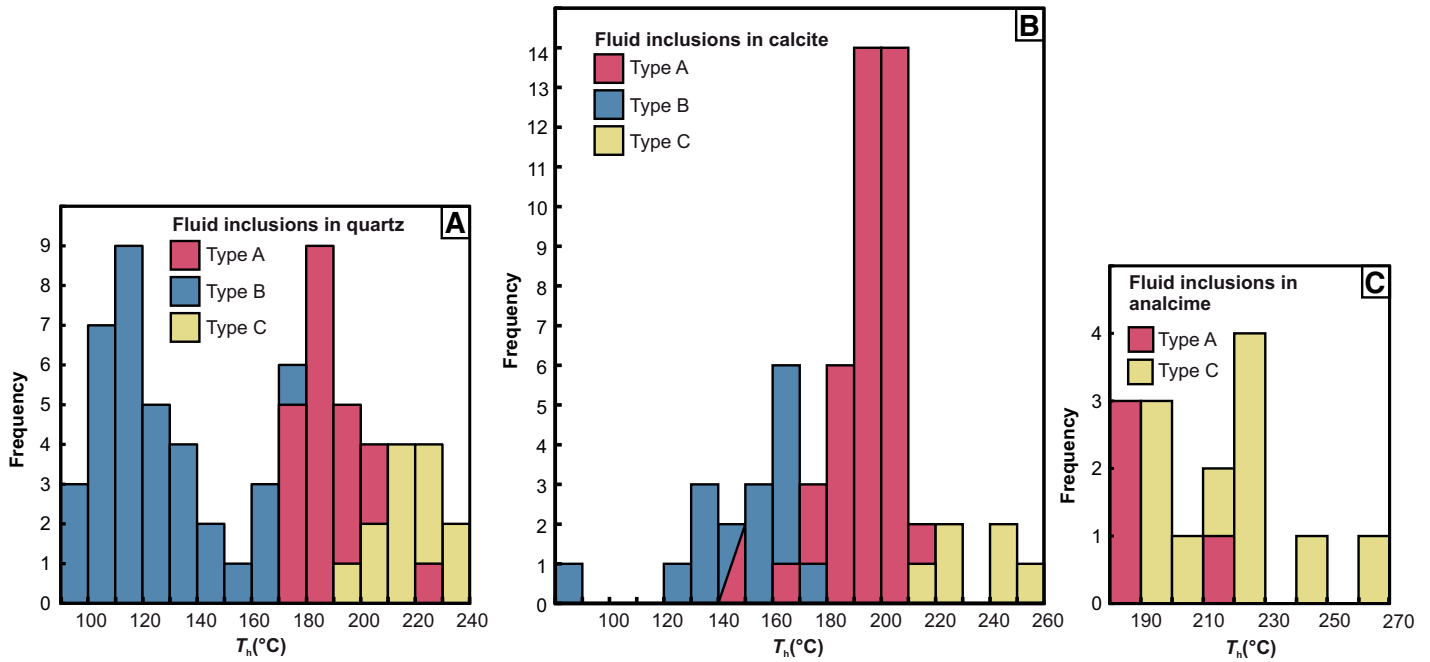


Figure 6. Histograms of type A, B, and C fluid inclusions in (A) quartz, (B) calcite, and (C) analcime.

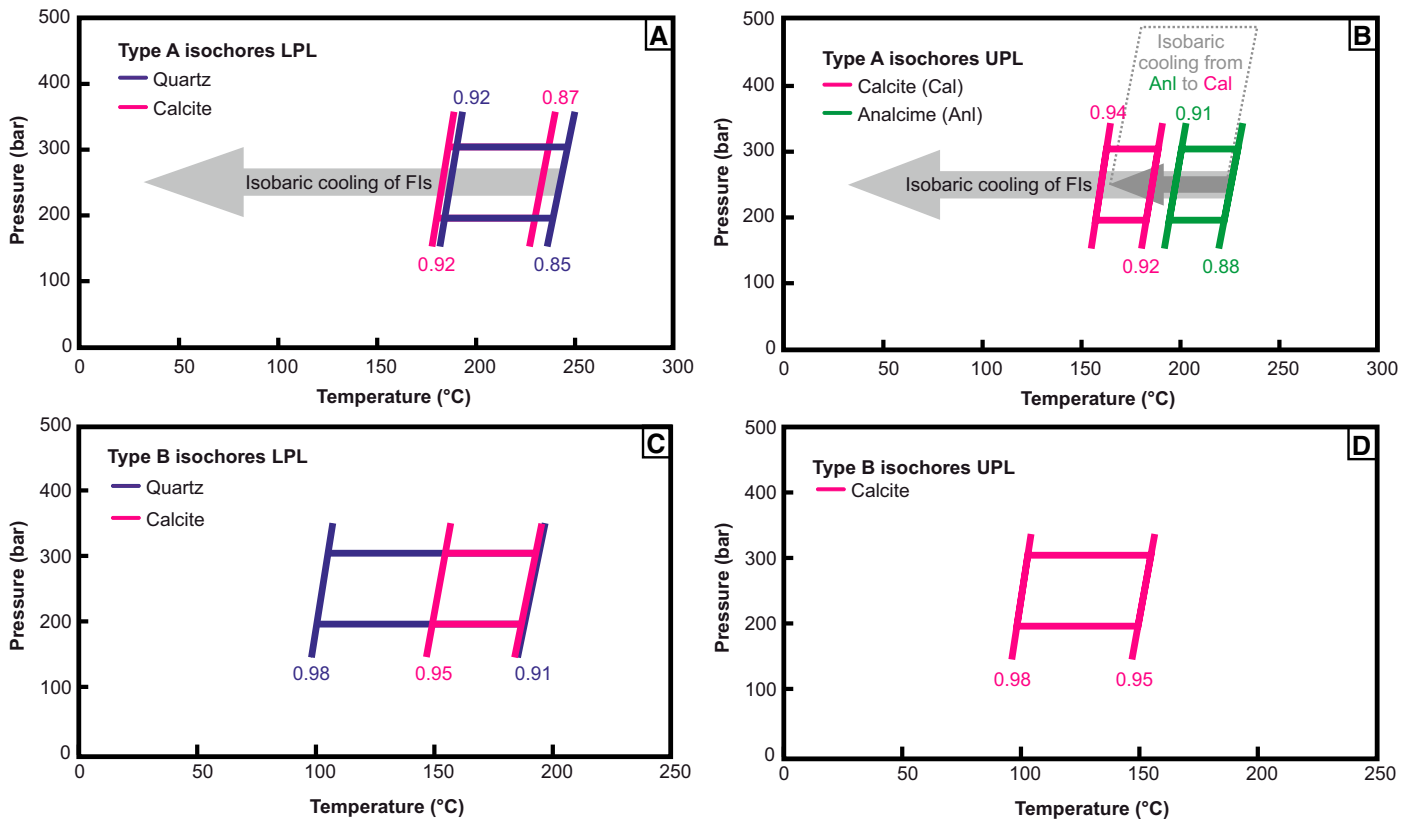


Figure 7. Calculated isochore fields of type A and type B fluid inclusions (FIs) in calcite, quartz, and analcime hosts from the Lower Pillow Lavas (LPL) and Upper Pillow Lavas (UPL). (A and B) Isochore fields of primary type A FIs entrapped in veins and vesicles from the LPL and UPL. (C and D) Isochore fields of secondary type B FIs entrapped in veins and vesicles from the LPL and UPL. Fields result from steep isochores from aqueous FIs crossed with minimum hydrostatic pressure. Gray arrows indicate isobaric cooling path. Numbers refer to FI densities of respective isochores in g/cm³. Anl—analcime; Cal—calcite.

in the estimated pressure range at around 210 °C (Fig. 7A). Conditions are representative for minimum entrapment temperatures of type A FIs. Due to almost comparable fluid inclusion densities and isochore fields of quartz and calcite, it is argued that these vein and vesicle minerals experienced similar formation conditions.

Analcime- and calcite-bearing syntaxial veins of the UPL host primary type A FIs that are distinguished by their isochore fields (Fig. 7B). FIs in analcime show some higher minimum temperature conditions compared to late-stage calcite from the same vein. This indicates growth of analcime followed by calcite and suggests mineral precipitation under conditions of almost isobaric cooling. Petrographic observations support this chronology of precipitation (Fig. 2D).

Isochore fields of secondary type B FIs entrapped in calcite and quartz from the LPL and UPL show a slight overlap with corresponding type A isochores but extend toward lower temperatures (i.e., higher densities up to 0.98 g/cm³) (Figs. 7C and 7D).

Type C FIs are interpreted as former large type A FIs that re-equilibrated and decrepitated due to isobaric cooling (Figs. 7A and 7B). Alternatively, ongoing pillow lava emplacement on top of the veined volcanic pile and nearby active feeder dykes may have had the potential to conductively reheat minerals and their fluid inclusions. Thus, isobaric heating may also explain the observed FI re-equilibration/decrepitation textures. However, the complete lack of typical secondary minerals indicative of slightly higher temperatures (~200–300 °C; e.g., chlorite, epidote, prehnite) (Kristmannsdóttir, 1979; Beaufort et al., 1992) in the LPL and UPL suggests that peak homogenization temperatures (up to 230 °C in quartz, Fig. 6A) have at least not been significantly exceeded. We therefore conclude a rather simple isobaric cooling scenario that is moreover characterized by isochores and petrography of analcime and late-stage calcite from the same syntaxial vein (Figs. 7B and 2D). The spatial distribution of FI re-equilibration/decrepitation textures in the Troodos area independently of host minerals (calcite and quartz) and vein types indicates isobaric cooling that affected the entire Troodos oceanic crust before uplift. Based on the present data, however, the timing of isobaric cooling (FI re-equilibration/decrepitation and formation of calcite after analcime in syntaxial veins) cannot be constrained in more detail. We favor an evolution, which was initiated by isobaric cooling of early to late syntaxial vein precipitates in the UPL and continued over a more extended time and temperature range that finally resulted in FI modifications within the UPL and LPL (Figs. 7A and 7B).

Mechanisms for Vein Mineral Precipitation and Fluid Flow

The occurrence of quartz and zeolites with high Si/Al ratios (mordeinite: 5, heulandite: 2.8–4) (Khodabandeh and Davis, 1996) is restricted to the silica supersaturated LPL and indicates that the chemical composition of the host rock is a crucial factor for mineralogy of vein precipitates. In contrast, veins within the basaltic and boninitic UPL bear calcite and zeolites with low Si/Al ratios (analcime: 2–2.5, natrolite: 1.5) (Chiperá and Apps, 2001).

The dominant fluid system during vein formation is inferred from FIs that indicate a simplified H₂O-NaCl ± KCl ± MgCl₂ chemistry, independent of the host mineral. Regarding microtextures, syntaxial and blocky veins give evidence for advective fluid flow through fractures in an open system. Early-stage quartz, detached from vein walls and located between grain boundaries of late-stage calcite, argues additionally for destructive fluid flow. Oscillatory growth zoning of late-stage calcite in cavities of incompletely sealed syntaxial veins points to a change into pervasive porous flow or even diffusion through host rock and vein minerals. A pure diffusive regime is proposed for antitaxial fibrous calcite veins (Means and Li, 2001; Bons et al., 2012). The fine nature of zonation in late-stage

calcite can be related to geochemical self-organization of a Mn-bearing fluid in a closed system. Furthermore, the presence of Mn decreases the precipitation rate and modifies the crystal lattice and its vacancies (Meyer, 1984; Dromgoole and Walter, 1987; Reeder et al., 1990). This modification enables the entrapment of numerous large fluid inclusions, which are susceptible to re-equilibration and decrepitation, considering a non-isochoric *P-T* evolution (e.g., isobaric cooling and/or isothermal decompression) (Vityk and Bodnar, 1995). This explains the coincidence of high-luminescent growth domains with high accumulations of decrepitation textures in blocky and elongate-blocky calcite (Figs. 4A and 4D). Syntaxial veins differ by their degree of sealing that is determined by the ratio between mineral growth and fracture opening. In incompletely sealed syntaxial veins fracture opening exceeds mineral growth rate and results in growth within a fluid-filled space, whereas completely sealed syntaxial veins are characterized by almost equal rates between mineral growth and fracture opening (Fisher and Brantley, 1992). The latter also represents a crack and sealing process (Ramsay, 1980; Bons et al., 2012).

Tectonic Implications—Modeling Vein Precipitation in a SSZ Setting

The mineralogy and high formation temperatures of veins investigated in this study are distinct from uplift-related gypsum and palygorskite veins within the UPL (Gillis and Robinson, 1990) that usually form at lower temperatures (<100 °C) (Church and Velde, 1979; Garcia-Ruiz et al., 2007). Therefore, the studied veins are probably related to pre-uplift processes.

Syntaxial veins are the most common vein type and are distributed throughout the whole volcanic sequence (Figs. 2A–2F). They can be related to mode I fractures after Bons et al. (2012), i.e., extensional gashes, characteristic for a tectonic origin. In contrast, blocky veins (Figs. 2G–2I) are associated with brecciated host rocks. They are interpreted as hydrofractures associated with fluid overpressure and prevent a tectonic origin (Bons et al., 2012). Antitaxial fibrous veins (Figs. 2J–2L) result from enhanced crystallization processes and are not related to tectonic processes (Taber, 1916; Means and Li, 2001). Fiber curvature points to changing stress orientations or rotations within the stress field during growth. Solid inclusion bands in these antitaxial fibrous veins most likely document changes in fluid chemistry rather than multiple crack and sealing processes.

Subduction initiation linked with slab-rollback has a significant extensional component. Slow spreading ridges like the Troodos SSZ are in particular associated with tectonic extension and normal faulting compared to fast spreading ridges like the Semail SSZ (Pearce et al., 1984; Dilek and Eddy, 1992; Mutter and Karson, 1992; Searle and Cox, 1999; Abelson et al., 2001; Dilek and Furnes, 2009). Hence, syntaxial veins, which are the most common vein type in the whole lava pile, may have a tectonic origin and can be linked with this extensional component.

A tectonic sketch explains formation and precipitation processes of the different studied vein types together with FI evolution in the proto-fore-arc setting of the N-S striking Troodos SSZ (Pearce et al., 1984; Maffione et al., 2017) exemplarily for the UPL (Fig. 8): Completely sealed syntaxial veins suffered fracturing and subsequent seawater infiltration accompanied by immediate mineral precipitation (crack and sealing process, Fig. 8A). Incompletely sealed syntaxial veins underwent fast opening rates and comparatively slow mineral growth rates (Figs. 8C and 8D). Late-stage minerals filled open cavities and mark a change from an open into a closed system that is characterized by geochemical self-organization (Fig. 8E). FIs entrapped in host minerals of both syntaxial vein types underwent isobaric cooling that finally resulted in re-equilibration and decrepitation of especially large-scale FIs (Figs. 8B and 8F). Blocky veins are associated with host rock brecciation and subsequent mineralization (Figs. 8G

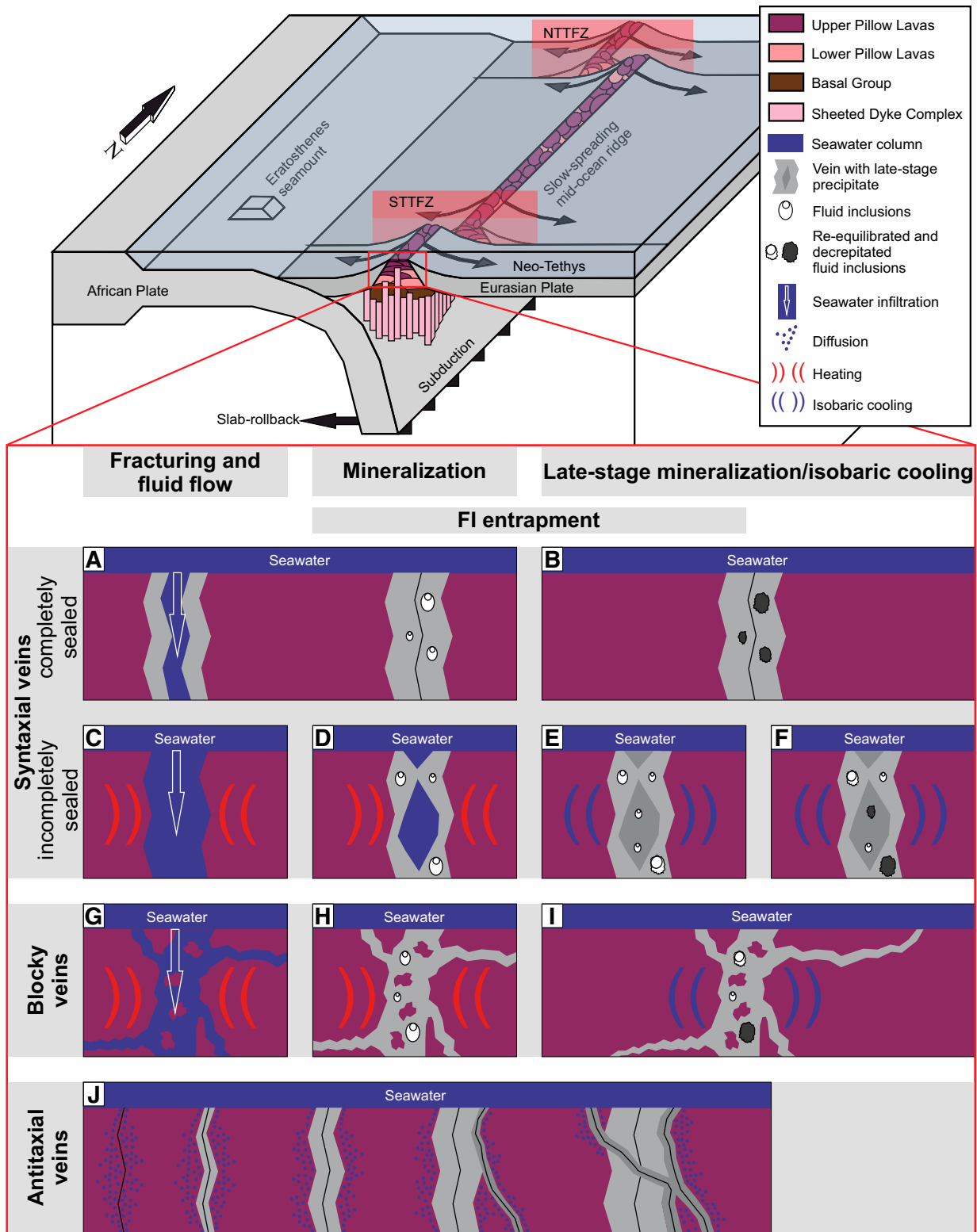


Figure 8. Tectonic sketch of the Troodos supra-subduction zone (SSZ) presenting a model for multiple vein mineral precipitation and fluid inclusion (FI) evolution exemplarily for the Upper Pillow Lavas. Veining of the Lower Pillow Lavas occurred analogously. Spreading axis strikes N-S parallel to the subduction zone and is bounded by the Northern (NTTFZ) and the Southern Troodos Transform Fault Zone (STTFZ). (A and B) Model for completely and (C–F) incompletely sealed syntaxial veins; (G–I) model for blocky veins with mineral precipitation after brecciation; (J) antitaxial veins as a result of diffusion-crystallization processes. (E) Late-stage precipitates in incompletely sealed syntaxial veins indicate initial isobaric cooling that continues over a more extended temperature and time range (B, F, and I) resulting in decrepitation and local re-equilibration of FIs in syntaxial and blocky veins. FIs in antitaxial veins lack or are insufficiently small.

and 8H). Entrapment of FIs and their re-equilibration and decrepitation are comparable to syntaxial veins (Fig. 8I). In both blocky and syntaxial veins, the host rock delivered the heat to increase the temperature of the pervading seawater. In antitaxial veins, fracturing is caused by mineral precipitation due to diffusion (Fig. 8J). FIs in this vein type are insufficiently small.

CONCLUSIONS

Previous studies on secondary minerals in the Troodos Pillow Lava sequence provide insights into temperature and chemical conditions during formation but give no information on vein mineral growth (Gillis and Robinson, 1985, 1990; Staudigel et al., 1986). This study deals with veins that reveal microtextures that are (1) possibly related to tectonic extension (syntaxial veins), (2) originated from hydrofracturing (blocky veins), and (3) formed due to diffusion-crystallization processes (antitaxial veins). The syntaxial veins are in good agreement with the typical tectonic regime observed in proto-fore-arcs within supra-subduction zones. This area is dominated by extension and associated with slow spreading rates in combination with a potential subduction initiation-coupled slab-rollback (Pearce et al., 1984; Dilek and Eddy, 1992; Mutter and Karson, 1992; Searle and Cox, 1999; Abelson et al., 2001; Dilek and Furnes, 2009).

The chemical composition of the host rock is the crucial factor for the vein mineralogy as also observed in the case of low-temperature alteration minerals of the Troodos ophiolite (Gass and Smewing, 1973; Gillis and Robinson, 1985, 1990). Initial mineral precipitation in fractures took place in an open system with advective fluid flow but changed later after incomplete sealing into a closed system characterized by geochemical self-organization (growth zoned late-stage calcite). Antitaxial fibrous veins give additionally a clear evidence for a diffusive regime.

Consistent T_m and T_h of calcite, quartz, and analcime veins (T_h from 180 to 210 °C) suggest precipitation from seawater shortly after pillow lava crystallization that agrees with earlier studies by Spooner and Bray (1977) and Staudigel et al. (1986).

Isobaric cooling of the entire Troodos oceanic crust resulted in re-equilibration and decrepitation of former large FIs entrapped in Mn-rich growth zones that facilitate their modification. These results from veins throughout the Troodos ophiolite are independent of mineralogy as well as spatial or stratigraphic units and argue for a Troodos-wide coherent isobaric cooling process that preceded the uplift of the Troodos ophiolite.

ACKNOWLEDGMENTS

This study was funded by the Austrian Science Fund (FWF-P 27982-N29). We thank two anonymous reviewers and the editor for their constructive comments.

REFERENCES CITED

Abelson, M., Baer, G., and Agnon, A., 2001, Evidence from gabbro of the Troodos ophiolite for lateral magma transport along a slow-spreading mid-ocean ridge: *Nature*, v. 409, no. 6816, p. 72–75, <https://doi.org/10.1038/35051058>.

Anonymous, 1972, Penrose field conference on ophiolites: *Geotimes*, v. 17, p. 24–25.

Bagnall, P.S., 1960, The geology and mineral resources of the Pano Lefkara-Larnaca area: Cyprus, Geological Survey Department, Memoir 5, 116 p.

Bakker, R.J., 1997, Clathrates: Computer programs to calculate fluid inclusion V–X properties using clathrate melting temperatures: *Computers & Geosciences*, v. 23, p. 1–18, [https://doi.org/10.1016/S0098-3004\(96\)00073-8](https://doi.org/10.1016/S0098-3004(96)00073-8).

Bakker, R.J., 2003, Package FLUIDS 1 Computer programs for analysis of fluid inclusion data and for modelling bulk fluid properties: *Chemical Geology*, v. 194, p. 3–23, [https://doi.org/10.1016/S0009-2541\(02\)00268-1](https://doi.org/10.1016/S0009-2541(02)00268-1).

Bear, L.M., 1960, The geology and mineral resources of the Akaki-Lythrodondha area: Cyprus, Geological Survey Department, Memoir 3, 122 p.

Bear, L.M., and Morel, S.W., 1960, The geology and mineral resources of the Agros-Akrotiri area: Cyprus, Geological Survey Department, Memoir 7, 88 p.

Beaufort, D., Patrier, P., Meunier, A., and Ottaviani, M.M., 1992, Chemical variations in assemblages including epidote and/or chlorite in the fossil hydrothermal system of Saint Martin (Lesser Antilles): *Journal of Volcanology and Geothermal Research*, v. 51, no. 1–2, p. 95–114, [https://doi.org/10.1016/0377-0273\(92\)90062-1](https://doi.org/10.1016/0377-0273(92)90062-1).

Bednarz, U., and Schmincke, H.U., 1994, Petrological and chemical evolution of the north-eastern Troodos Extrusive Series, Cyprus: *Journal of Petrology*, v. 35, no. 2, p. 489–523, <https://doi.org/10.1093/petrology/35.2.489>.

Bodnar, R.J., 2003, Introduction to aqueous-electrolyte fluid inclusions, in Samson, I., Anderson, A., and Marshall, D., eds., *Fluid Inclusions: Analysis and Interpretations: Mineralogical Association of Canada Short Course*, v. 32, p. 81–100.

Bons, P.D., and Montenari, M., 2005, The formation of antitaxial calcite veins with well-developed fibres, Oppaminda Creek, South Australia: *Journal of Structural Geology*, v. 27, no. 2, p. 231–248, <https://doi.org/10.1016/j.jsg.2004.08.009>.

Bons, P.D., Elburg, M.A., and Gomez-Rivas, E., 2012, A review of the formation of tectonic veins and their microstructures: *Journal of Structural Geology*, v. 43, p. 33–62, <https://doi.org/10.1016/j.jsg.2012.07.005>.

Burkhard, M., 1993, Calcite twins, their geometry, appearance and significance as stress-strain markers and indicators of tectonic regime: A review: *Journal of Structural Geology*, v. 15, no. 3–5, p. 351–368, [https://doi.org/10.1016/0191-8141\(93\)90132-T](https://doi.org/10.1016/0191-8141(93)90132-T).

Cameron, W.E., Nisbet, E.G., and Dietrich, V.J., 1979, Boninites, komatiites and ophiolitic basalts: *Nature*, v. 280, 5723, p. 550–553, <https://doi.org/10.1038/280550a0>.

Carr, J.M., and Bear, L.M., 1960, The geology and mineral resources of the Peristerona-Lagouthera area: Cyprus, Geological Survey Department, Memoir 2, 79 p.

Chiper, S.J., and Apps, L.M., 2001, Geochemical stability of natural zeolites: *Reviews in Mineralogy and Geochemistry*, v. 45, no. 1, p. 117–161, <https://doi.org/10.2138/rmg.2001.45.3>.

Church, T.M., and Velde, B., 1979, Geochemistry and origin of a deep-sea Pacific palysgorskite deposit: *Chemical Geology*, v. 25, no. 1–2, p. 31–39, [https://doi.org/10.1016/0009-2541\(79\)90081-0](https://doi.org/10.1016/0009-2541(79)90081-0).

Clube, T.M.M., Creer, K.M., and Robertson, A.H.F., 1985, Palaeorotation of the Troodos microplate, Cyprus: *Nature*, v. 317, 6037, p. 522–525, <https://doi.org/10.1038/317522a0>.

Constantinou, C., 1995, Geological Map of Cyprus: Cyprus, Geological Survey Department, scale 1:250,000, 1 sheet.

Dilek, Y., and Eddy, C.A., 1992, The Troodos (Cyprus) and Kizildag (S. Turkey) ophiolites as structural models for slow-spreading ridge segments: *The Journal of Geology*, v. 100, no. 3, p. 305–322, <https://doi.org/10.1086/629634>.

Dilek, Y., and Flower, M.F., 2003, Arc-trench rollback and forearc accretion: 2. A model template for ophiolites in Albania, Cyprus, and Oman, in Dilek, Y., and Robinson, P.T., eds., *Ophiolites in Earth History: Geological Society, London, Special Publication 218*, no. 1, p. 43–68, <https://doi.org/10.1144/GSL.SP.2003.218.01.04>.

Dilek, Y., and Furnes, H., 2009, Structure and geochemistry of Tethyan ophiolites and their petrogenesis in subduction rollback systems: *Lithos*, v. 113, no. 1, p. 1–20, <https://doi.org/10.1016/j.lithos.2009.04.022>.

Dromgoole, E.L., and Walter, L.M., 1987, Iron and manganese incorporation into calcite cements: Implications for diagenetic studies: *Geological Society of America Abstracts with Programs*, v. 19, no. 7, p. 647.

Fairchild, I.J., 1983, Chemical controls of cathodoluminescence of natural dolomites and calcites: *New data and review: Sedimentology*, v. 30, no. 4, p. 579–583, <https://doi.org/10.1111/j.1365-3091.1983.tb00695.x>.

Fisher, D.M., and Brantley, S.L., 1992, Models of quartz overgrowth and vein formation: deformation and episodic fluid flow in an ancient subduction zone: *Journal of Geophysical Research, Solid Earth*, v. 97, B13, p. 20,043–20,061, <https://doi.org/10.1029/92JB01582>.

García-Ruiz, J.M., Villasuso, R., Ayora, C., Canals, A., and Otálora, F., 2007, Formation of natural gypsum megacrystals in Naica, Mexico: *Geology*, v. 35, no. 4, p. 327–330, <https://doi.org/10.1130/G23393A.1>.

Gass, I.G., 1960, The geology and mineral resources of the Dhali area: Cyprus, Geological Survey Department Memoir 4, 116 p.

Gass, I.G., 1968, Is the Troodos massif of Cyprus a fragment of Mesozoic ocean floor?: *Nature*, v. 220, p. 39–42, <https://doi.org/10.1038/220039a0>.

Gass, I.G., and Masson-Smith, D., 1963, The geology and gravity anomalies of the Troodos Massif, Cyprus: *Philosophical Transactions of the Royal Society of London A: Mathematical: Physical and Engineering Sciences*, v. 255, no. 1060, p. 417–467, <https://doi.org/10.1098/rsta.1963.0009>.

Gass, I.G., and Smewing, J.D., 1973, Intrusion, extrusion and metamorphism at constructive margins: Evidence from the Troodos Massif, Cyprus: *Nature*, v. 242, 5392, p. 26–29, <https://doi.org/10.1038/242026a0>.

Gillis, K.M., and Robinson, P.T., 1985, Low-temperature alteration of the extrusive sequence, Troodos ophiolite, Cyprus: *Canadian Mineralogist*, v. 23, p. 431–441.

Gillis, K.M., and Robinson, P.T., 1990, Patterns and processes of alteration in the lavas and dykes of the Troodos ophiolite, Cyprus: *Journal of Geophysical Research, Solid Earth*, v. 95, B13, p. 21,523–21,548, <https://doi.org/10.1029/JB095iB13p21523>.

Goldstein, R.H., and Reynolds, T.J., eds., 1994, Systematics of fluid inclusions in diagenetic minerals: *Society for Sedimentary Geology, SEPM Short Course 31*, p. 199, <https://doi.org/10.2110/scn.94.31>.

Khodabandeh, S., and Davis, M.E., 1996, Synthesis of a heulandite-type zeolite by hydrothermal conversion of zeolite P1: *Chemical Communications*, v. 10, p. 1205–1206, <https://doi.org/10.1039/cc9960001205>.

Knight, C.L., Williamson, M.A., and Bodnar, R.J., 1989, Raman spectroscopy of zeolites: Characterization of natural zeolites with the laser Raman microprobe: *Microbeam Analysis*, v. 1989, p. 571–573.

Kristmannsdóttir, H., 1979, Alteration of basaltic rocks by hydrothermal-activity at 100–300 °C: Developments in *Sedimentology*, v. 27, p. 359–367, [https://doi.org/10.1016/S0070-4571\(08\)70732-5](https://doi.org/10.1016/S0070-4571(08)70732-5).

MacLeod, C.J., and Murton, B.J., 1993, Structure and tectonic evolution of the Southern Troodos transform fault zone, Cyprus, in Prichard, H.M., Alabaster, T., Harris, N.B.W., and Neary, C.R., eds., *Magmatic Processes and Plate Tectonics: Geological Society, London, Special Publication 76*, p. 141–176.

- Maffione, M., Hinsbergen, D.J., Gelder, G.J., Goes, F.C., and Morris, A., 2017, Kinematics of Late Cretaceous subduction initiation in the Neo-Tethys Ocean reconstructed from ophiolites of Turkey, Cyprus, and Syria: *Journal of Geophysical Research, Solid Earth*, v. 122, no. 5, p. 3953–3976, <https://doi.org/10.1002/2016JB013821>.
- Means, W.D., and Li, T., 2001, A laboratory simulation of fibrous veins: Some first observations: *Journal of Structural Geology*, v. 23, no. 6, p. 857–863, [https://doi.org/10.1016/S0191-8141\(00\)00158-9](https://doi.org/10.1016/S0191-8141(00)00158-9).
- Meyer, H.J., 1984, The influence of impurities on the growth rate of calcite: *Journal of Crystal Growth*, v. 66, no. 3, p. 639–646, [https://doi.org/10.1016/0022-0248\(84\)90164-7](https://doi.org/10.1016/0022-0248(84)90164-7).
- Miyashiro, A., 1973, The Troodos ophiolitic complex was probably formed in an island arc: *Earth and Planetary Science Letters*, v. 19, no. 2, p. 218–224, [https://doi.org/10.1016/0012-821X\(73\)90118-0](https://doi.org/10.1016/0012-821X(73)90118-0).
- Moore, E.M., and Vine, F.J., 1971, The Troodos Massif, Cyprus and other ophiolites as oceanic crust: Evaluation and implications: *Philosophical Transactions of the Royal Society of London A: Mathematical, Physical and Engineering Sciences*, v. 268, no. 1192, p. 443–467, <https://doi.org/10.1098/rsta.1971.0006>.
- Morris, A., and Maffione, M., 2016, Is the Troodos ophiolite (Cyprus) a complete, transform fault-bounded Neotethyan ridge segment?: *Geology*, v. 44, no. 3, p. 199–202, <https://doi.org/10.1130/G37529.1>.
- Morris, A., Creer, K.M., and Robertson, A.H.F., 1990, Palaeomagnetic evidence for clockwise rotations related to dextral shear along the Southern Troodos Transform Fault, Cyprus: *Earth and Planetary Science Letters*, v. 99, no. 3, p. 250–262, [https://doi.org/10.1016/0012-821X\(90\)90114-D](https://doi.org/10.1016/0012-821X(90)90114-D).
- Mukasa, S.B., and Ludden, J.N., 1987, Uranium-lead isotopic ages of plagiogranites from the Troodos ophiolite, Cyprus, and their tectonic significance: *Geology*, v. 15, no. 9, p. 825–828, [https://doi.org/10.1130/0091-7613\(1987\)15<825:UIAOPF>2.0.CO;2](https://doi.org/10.1130/0091-7613(1987)15<825:UIAOPF>2.0.CO;2).
- Mutter, J., and Karson, J., 1992, Structural processes at slow-spreading ridges: *Science*, v. 257, 5070, p. 627–634, <https://doi.org/10.1126/science.257.5070.627>.
- Osozawa, S., Shinjo, R., Lo, C.H., Jahn, B.M., Hoang, N., Sasaki, M., Ishikawa, K.L., Kano, H., Hishi, H., Xenophontos, C., and Wakabayashi, J., 2012, Geochemistry and geochronology of the Troodos ophiolite: An SSZ ophiolite generated by subduction initiation and an extended episode of ridge subduction?: *Lithosphere*, v. 4, no. 6, p. 497–510, <https://doi.org/10.1130/L205.1>.
- Pearce, J.A., Lippard, S.J., and Roberts, S., 1984, Characteristics and tectonic significance of supra-subduction zone ophiolites: Geological Society, London, Special Publication 16, no. 1, p. 77–94, <https://doi.org/10.1144/GSL.SR1984.016.01.06>.
- Pearce, J.A., 2003, Supra-subduction zone ophiolites: The search for modern analogues, in Dilek, Y., and Newcomb, S., eds., *Ophiolite Concept and the Evolution of Geological Thought*: Boulder, Colorado: Geological Society of America. Special Paper, 373, p. 269–293.
- Pearce, J.A., and Robinson, P.T., 2010, The Troodos ophiolitic complex probably formed in a subduction initiation, slab edge setting: *Gondwana Research*, v. 18, no. 1, p. 60–81, <https://doi.org/10.1016/j.gr.2009.12.003>.
- Ramsay, J.G., 1980, The crack-seal mechanism of rock deformation: *Nature*, v. 284, p. 135–139, <https://doi.org/10.1038/284135a0>.
- Rautenschlein, M., Hofmann, A.W., Jenner, G.A., and Schmincke, H.U., 1985a, Troodos ophiolite: Implications for the mantle source: *Eos*, v. 66, p. 1123.
- Rautenschlein, M., Jenner, G.A., Hertogen, J., Hofmann, A.W., Kerrich, R., Schmincke, H.U., and White, W.M., 1985b, Isotopic and trace element composition of volcanic glasses from the Akaki Canyon, Cyprus: Implications for the origin of the Troodos ophiolite: *Earth and Planetary Science Letters*, v. 75, no. 4, p. 369–383, [https://doi.org/10.1016/0012-821X\(85\)90180-3](https://doi.org/10.1016/0012-821X(85)90180-3).
- Reeder, R.J., Fagioli, R.O., and Meyers, W.J., 1990, Oscillatory zoning of Mn in solution-grown calcite crystals: *Earth-Science Reviews*, v. 29, no. 1–4, p. 39–46, [https://doi.org/10.1016/0012-8252\(0\)90026-R](https://doi.org/10.1016/0012-8252(0)90026-R).
- Robertson, A.H.F., 1977, Tertiary uplift history of the Troodos massif, Cyprus: *Geological Society of America Bulletin*, v. 88, no. 12, p. 1763–1772, [https://doi.org/10.1130/0016-7606\(1977\)88<1763:TUHOTT>2.0.CO;2](https://doi.org/10.1130/0016-7606(1977)88<1763:TUHOTT>2.0.CO;2).
- Robertson, A.H.F., 1998, Tectonic significance of the Eratosthenes Seamount: A continental fragment in the process of collision with a subduction zone in the eastern Mediterranean (Ocean Drilling Program Leg 160): *Tectonophysics*, v. 298, no. 1, p. 63–82, [https://doi.org/10.1016/S0040-1951\(98\)00178-4](https://doi.org/10.1016/S0040-1951(98)00178-4).
- Robinson, P.T., Melson, W.G., O'Hearn, T., and Schmincke, H.U., 1983, Volcanic glass compositions of the Troodos ophiolite, Cyprus: *Geology*, v. 11, no. 7, p. 400–404, [https://doi.org/10.1130/0091-7613\(1983\)11<400:VGCOTT>2.0.CO;2](https://doi.org/10.1130/0091-7613(1983)11<400:VGCOTT>2.0.CO;2).
- Schmincke, H.U., Rautenschlein, M., Robinson, P.T., and Mehegan, J.M., 1983, Troodos extrusive series of Cyprus: A comparison with oceanic crust: *Geology*, v. 11, no. 7, p. 405–409, [https://doi.org/10.1130/0091-7613\(1983\)11<405:TESOCA>2.0.CO;2](https://doi.org/10.1130/0091-7613(1983)11<405:TESOCA>2.0.CO;2).
- Sclater, J.G., Anderson, R.N., and Bell, M.L., 1971, Elevation of ridges and evolution of the central eastern Pacific: *Journal of Geophysical Research*, v. 76, no. 32, p. 7888–7915, <https://doi.org/10.1029/JB076i032p07888>.
- Searle, M., and Cox, J., 1999, Tectonic setting, origin, and obduction of the Oman ophiolite: *Geological Society of America Bulletin*, v. 111, no. 1, p. 104–122, [https://doi.org/10.1130/0016-7606\(1999\)111<0104:TSAOAO>2.3.CO;2](https://doi.org/10.1130/0016-7606(1999)111<0104:TSAOAO>2.3.CO;2).
- Spooner, E.T.C., 1980, Cu-pyrite mineralization and seawater convection in oceanic crust: the ophiolitic ore deposits of Cyprus, in Strangway, D.W., ed., *The Continental Crust and Its Mineral Deposits*: Geological Association of Canada Special Paper 20, p. 685–704.
- Spooner, E.T.C., and Bray, C.J., 1977, Hydrothermal fluids of seawater salinity in ophiolitic sulfide ore deposits in Cyprus: *Nature*, v. 266, p. 808–812, <https://doi.org/10.1038/266808a0>.
- Staudigel, H., Gillis, K., and Duncan, R., 1986, K/Ar and Rb/Sr ages of celadonites from the Troodos ophiolite, Cyprus: *Geology*, v. 14, no. 1, p. 72–75, [https://doi.org/10.1130/0091-7613\(1986\)14<72:AASAO>2.0.CO;2](https://doi.org/10.1130/0091-7613(1986)14<72:AASAO>2.0.CO;2).
- Taber, S., 1916, The origin of veins of the asbestiform minerals: *Proceedings of the National Academy of Sciences of the United States of America*, v. 2, no. 12, p. 659–664, <https://doi.org/10.1073/pnas.2.12.659>.
- Thy, P., and Esbensen, K.H., 1993, Seafloor spreading and the ophiolitic sequences of the Troodos Complex: A principal component analysis of lava and dike compositions: *Journal of Geophysical Research, Solid Earth*, v. 98, B7, p. 11,799–11,805, <https://doi.org/10.1029/93JB00695>.
- van Everdingen, D.A., and Cawood, P.A., 1995, Dyke domains in the Mitsero graben, Troodos ophiolite, Cyprus: An off-axis model for graben formation at a spreading centre: *Journal of the Geological Society*, v. 152, no. 6, p. 923–932, <https://doi.org/10.1144/GSL.JGS.1995.152.01.07>.
- Vityk, M.O., and Bodnar, R.J., 1995, Textural evolution of synthetic fluid inclusions in quartz during reequilibration, with applications to tectonic reconstruction: *Contributions to Mineralogy and Petrology*, v. 121, no. 3, p. 309–323, <https://doi.org/10.1007/BF02688246>.
- Wilson, R.A.M., and Ingham, F.T., 1959, *The Geology of the Xeros-Troodos Area, with an Account of the Mineral Resources*: Ministry of Agriculture and Natural Resources: Geological Survey Department, Cyprus, Memoir 1, 135 p.

MANUSCRIPT RECEIVED 9 AUGUST 2017
 REVISED MANUSCRIPT RECEIVED 5 APRIL 2018
 MANUSCRIPT ACCEPTED 30 APRIL 2018